Luminescence, Patterned Metallic Regions, and Photon-Mediated Electronic Changes in Single-Sided Fluorinated Graphene Sheets

Andrew Leigh Walter,[†,‡,§,□,*] Hasan Sahin,[⊥] Ki-Joon Jeon,[∥] Aaron Bostwick,[†] Seyda Horzum,[⊥] Roland Koch,[⊗] Florian Speck,[⊗] Markus Ostler,[⊗] Peter Nagel,[#] Michael Merz,[#] Stefan Schupler,[#] Luca Moreschini,[†] Young Jun Chang,[△] Thomas Seyller,[▽] Francois M. Peeters,[⊥] Karsten Horn,[‡] and Eli Rotenberg[†]

[†]Advanced Light Source (ALS), E. O. Lawrence Berkeley National Laboratory, Berkeley, California 94720, United States, [‡]Department of Physical Chemistry, Fritz-Haber-Institut der Max-Planck-Gesellschaft, Faradayweg 4-6, 14195 Berlin, Germany, [§]Donostia International Physics Centre, Paseo Manuel de Lardizabal, 4, 20018 Donostia-San Sebastian, Spain, [⊥]Department of Physics, University of Antwerp, Groenenborgerlaan 171, B-2020 Antwerpen, Belgium, [∥]Department of Environmental Engineering, INHA University, Incheon 402-751, Korea, [⊗]Lehrstuhl für Technische Physik, Universität Erlangen-Nürnberg, Erwin-Rommel-Strasse 1, 91058 Erlangen, Germany, [#]Institut für Festkörperphysik, Karlsruhe Institute of Technology (KIT), 76344 Eggenstein-Leopoldshafen, Germany, [△]Department of Physics, University of Seoul, Seoul 130-743, Korea, and [▽]Institut für Physik, Technische Universität Chemnitz, 09126 Chemnitz, Germany. [□]Present address: Photon Sciences Directorate, Brookhaven National Laboratory, NSLS II, Upton, New York 11973, United States.

ABSTRACT Single-sided fluorination has been predicted to open an electronic band gap in graphene and to exhibit unique electronic and magnetic properties; however, this has not been substantiated by experimental reports. Our comprehensive experimental and theoretical study of this material on a SiC(0001) substrate shows that single-sided fluorographene exhibits two phases, a stable one with a band gap of ~6 eV and a metastable one, induced by UV irradiation, with a band gap of ~2.5 eV. The metastable structure, which reverts to the stable "ground-state" phase upon annealing under emission of blue light, in our view is induced by defect states, based on the observation of a nondispersive electronic state at the top of the valence band, not unlike that found in organic molecular layers. Our structural data show that the stable C2F ground state has a "boat" structure, in agreement with our X-ray magnetic circular dichroism data, which show the absence of an ordered magnetic phase. A high flux of UV or X-ray photons removes the fluorine atoms, demonstrating the possibility of lithographically patterning conducting regions into an otherwise semiconducting 2D material.

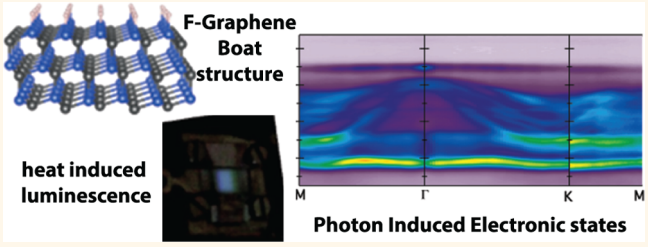

KEYWORDS: graphene · fluorine · photoemission · XMCD · STM

The interest in graphene, a single layer of hexagonally coordinated carbon atoms, has been exponentially increasing in recent years, not only because of the interesting physical properties arising from its "massless Dirac fermion" charge carriers[1−6] but also because of the promise of novel electronic devices that may be realized from this material.[1,7−10] However, the absence of a sizable fundamental band gap has limited the scope for applications. Some progress has been made in this respect by oxidizing graphene sheets, which produce a band gap on the order of 5 eV tunable by varying the amount of oxidation;[11] however, the structural order does not extend beyond a few C−C bond distances, and this material also has a finite density of states at the Fermi level, detrimental to electronic applications. Hydrogenated graphene (graphane) suffers from similar problems and has a low stability even at moderate temperatures.[12] The search for a suitable graphene derivative that exhibits a sizable band gap has thus turned to fluorinated graphene (fluorographene). Complete fluorination, where each carbon atom is bonded to a fluorine atom (*i.e.*, a 2D counterpart of Teflon) has been shown[13−15] to lead to a material with a

* Address correspondence to awalter@bnl.gov.

Received for review February 27, 2014 and accepted August 8, 2014.

Published online August 08, 2014
10.1021/nn501163c

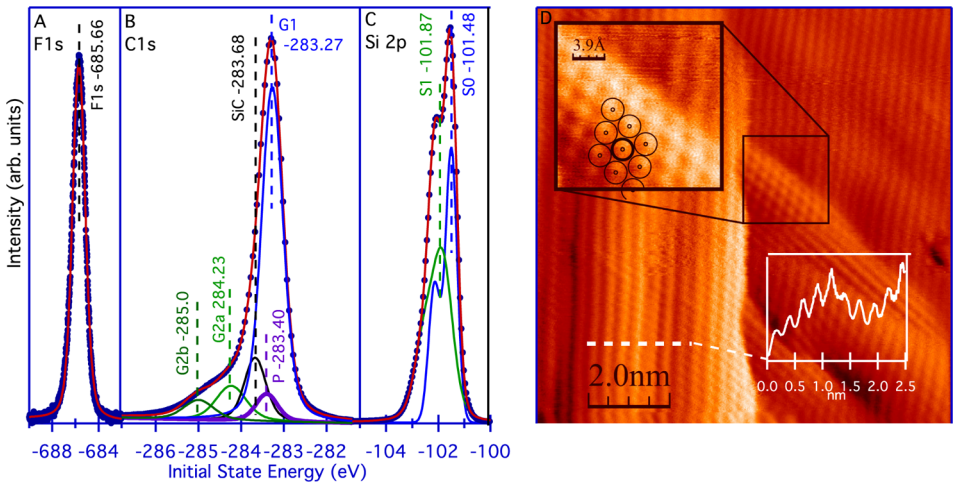

Figure 1. (A–C) X-ray photoelectron core level spectra obtained from a single-sided fluorinated graphene on H/SiC sample. The F 1s detail scan obtained using 900 eV photons indicates that only a single F species is present. The C 1s detail scan (B) obtained using 350 eV photons is composed of the substrate (SiC), 3 sp^3 (C–F bonded) carbon (G2a, G2b, and P), and an unfluorinated C (G1) component. The Si 2p (C) detail scans obtained using 350 eV photons are also similar to those found for pristine graphene on SiC and for H-terminated SiC,[24,28] indicating that the fluorine does not interact with the substrate. Blue circles are experimental data, colored lines are individual Lorentzian–Gaussian peaks fitted to the experimental data, and red lines are the fitted spectra. (D) Constant-current STM image (U_{bias} = 2.5 V, I_{tip} = 1 nA) from single-side fluorinated graphene on H/SiC. The white inset shows a line profile taken from the thick white line in D, indicating the 2.5 height oscillations.

large (~3 eV) band gap; however, while applications are envisaged,[13,15–19] a considerable lattice corrugation is expected, rendering this material less suitable for true 2D applications.

This drawback does not seem to exist in fluorographene, where only every second carbon atom is bonded to a fluorine atom on one side of the graphene, *i.e.*, a C_2F-like phase. This situation creates unsaturated p_z orbitals on the nonfluorinated side, leading to semiconducting valence and conduction bands of qualitatively different origin.[20–22] Here we show, using a large range of geometric and electronic structure investigation tools, that fluorination of graphene grown epitaxially on the silicon side of silicon carbide (*i.e.*, SiC(0001)) leads to fluorine–carbon bonds on a single side of graphene (hence single-sided fluorographene, S-FG), with a large band gap. Moreover, exposure to extreme ultraviolet (EUV) photons induces a metastable phase with a much smaller band gap; this phase reverts to the stable phase under (thermoluminescent) emission of blue light. In both phases, the density of states vanishes at the Fermi level. Fluorination may be completely removed by extremely high doses of EUV or X-rays, suggesting the application of standard lithographic techniques to create structures with adjacent conducting and insulating regions.

RESULTS AND DISCUSSION

The single-sided fluorinated graphene studied here was prepared from epitaxial graphene grown on SiC(0001)[23] and converted into quasi-freestanding graphene by hydrogen intercalation.[24] Samples were then exposed to XeF_2 in a reaction chamber at elevated temperatures (200 °C) for 3–4 h, a method previously used to study fluorine interaction with silicon and graphene surfaces[13,14,25–27] and shown to lead to the formation of C– F bonds with the graphene layer, as can be seen from the core level spectra in Figure 1A–C. The fluorine 1s line (Figure 1 A), which can be modeled by a single narrow component, was measured on the samples before and after each additional experiment (including STM, XMCD, LEED, and ARPES) to confirm the integrity of fluorine on the sample. The carbon 1s line (Figure 1B) has several contributions, from atoms bonded in various conformations. We assign the substrate (SiC) carbon peak to the component at 283.68 eV by comparing the spectra from Figure 1B (350 eV photons) with those recorded under more bulk sensitive conditions (900 eV photons). In this comparison peaks that increase with photon energy (*i.e.*, the one labeled SiC) are due to bulk atoms, while those that decrease (the remaining components) are due to surface-related features. This binding energy assignment compares well with the lines observed for hydrogen-intercalated SiC.[24,28] The second assignment is for the fluorinated carbon lines in the ground state (G2a and G2b) and the unfluorinated carbon (G1). This assignment is based on the expectation, from charge transfer arguments, that fluorinated carbon peaks will appear at higher energies. The assignment of the two peaks to the fluorinated carbon is also supported by the changes that occur with EUV exposure described in detail below; the G1 line intensity remains constant, while the G2a and G2b lines decrease in intensity. A corresponding increase in the line labeled P allows for the assignment of this peak to the metastable phase. The Si 2p peak is identical to the one reported for hydrogen-intercalated graphene on SiC,[24,28] indicating

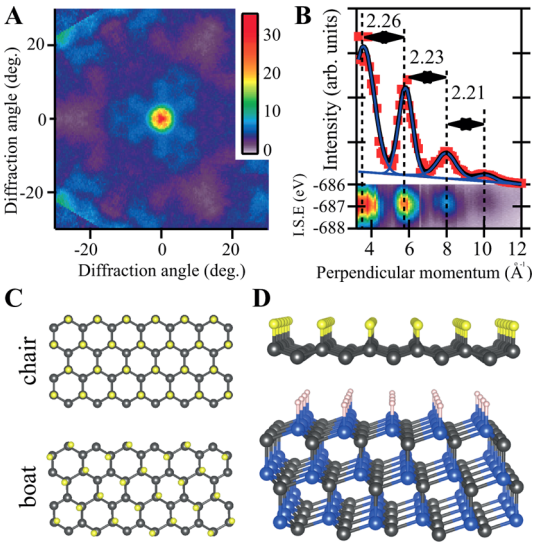

Figure 2. Photon energy dependent X-ray diffraction (CPD) pattern from the F 1s core level plotted in a nonlinear color scale, which highlights the weaker features. (B) Integrated intensity variation of the central spot as a function of photon energy, converted to perpendicular momentum (see text), with experimental data as dotted lines (red) and fitted Lorentzian−Gaussian peaks shown as solid (blue) lines. The binding energy resolved diffraction plot is presented in the lower panel of B. The average peak separation yields a carbon− fluorine bond length of 1.41 ± 0.015 Å. (C) Top view of chair and boat conformations of S-FG and (D) tilted view of boat S-FG on hydrogen-intercalated SiC(0001) with carbon atoms in black, fluorine in yellow, Si in blue, and H in pink.

that the substrate is not affected by the fluorination process.

In addition to the location of the XPS lines the relative intensities also provide important information about the sample. We have evaluated the area under the fitted peaks. In order to compare the F to C atomic ratio, calculated photoemission cross-section data[29] were used for normalization. Comparison of the F 1s line to the sum of all surface carbon peaks (G1, G2a, G2b, and P) gives a value of ~37% fluorination. On the basis of our assignment of the G2A, G2B, and P carbon lines to fluorinated carbon species, and comparing the area of these peaks to that of the G1 carbon line (non-fluorine-bonded carbon), a value of ~43% fluorination is determined. This discrepancy is most likely due to photoelectron diffraction effects that can strongly influence a quantitative evaluation of relative peak intensities (see Figure 2). The analysis of the STM data taken on these samples, discussed below, suggests that fluorination in our samples is 50%; hence all three coverage calibrations show that the samples have the C_2F structure. The significantly different XPS spectra recently observed for fully fluorinated graphene[13] compared to our XPS analysis support the conclusion that the current samples are C_2F not CF. It is important to note here that in our case we fluorinate the samples at 200 °C for 3−4 h, while Nair *et al.*[13] fluorinated the sample at 450 °C for 2 months, leading to a substantially different fluorinated structure.

The fluorination process gives rise to long-range ordered structures on the surface, as shown in the STM image in Figure 1D; it displays a ridge-like structure, with very small minority regions having a hexagonal lattice phase. Annealing of the samples prior to measurement ensures that we predominantly measure the ground-state phase (this process is documented below). We interpret the ridge-like structure to be formed by adjacent fluorine atoms separated from each other through valleys formed by fluorine-free carbon atoms, *i.e.*, in the "boat" phase depicted in Figure 2C and D. Within the limits of an analysis of STM topography, we measure a ridge−ridge distance of 2.51 Å, which compares well with the calculated value of 2.60 Å.

The minority hexagonal patterns can then be assigned either to the "chair" structure (also shown in Figure 2C and D), some unfluorinated regions, or a region of the "boat" structure with a significant amount of defects. In this picture these "hexagonal patterns" appear to occur at dislocation edges or other kinds of defects, as would be expected for the defect explanation. As mentioned above, the XPS analysis and the lack of strong contrast between the "hexagonal" and "ridge-like" regions in the STM strongly suggest that these are not regions of unfluorinated graphene. Below we discuss theoretical calculations that provide strong evidence that we do not have "chair" and "boat" regions in our samples; hence we assign the "hexagonal regions" to "defect regions" on the sample. As mentioned above, XPS and also ARPES and NEXAFS also show the existence of two phases, one of which (the "boat" ground state) can be converted into the metastable phase by illumination with extreme UV or X-ray photons.

We use X-ray photoelectron diffraction (XPD) to quantitatively determine the structure and bond length of S-FG. The fluorine 1s XPD pattern in Figure 2A shows a F 1s signal that is strongly concentrated along the surface normal, a fact that we interpret as being due to strong backscattering of electrons from the carbon atom directly underneath. The backscattering intensity as a function of photon energy (*i.e.*, wave vector normal to the surface) can then be used to precisely determine the carbon−fluorine bond length; when directly emitted and backscattered electrons are in phase, they constructively interfere and intensity is strongly enhanced. Varying the photon energy changes the phase condition and leads to a strong oscillation of the signal (Figure 2B) whose period is directly related to the bond length. (The photon energy range for the diffraction experiment was 730 to 1230 eV, and assuming an inner potential, V_{in}, of −16.5 eV[30] and the measured kinetic energy, E_k, the momentum normal to the surface can be evaluated *via* the relation $k_{normal} = (2me/\hbar^2(E_k - V_{in}))^{1/2}$.) The separation of the fitted peak positions in Figure 2B then gives a carbon−fluorine bond length of 1.41 ± 0.015 Å, consistent with that measured for C−F

intercalation compounds but somewhat shorter than those predicted by DFT calculations.[31]

Our interpretation of the diffraction patterns and the STM data below in terms of single-sided fluorographene in which the F atoms are bonded to every second carbon atom is supported by our DFT calculations for carbon−fluorine interaction, which show that the "chair" (see Figure 2C and D) conformation, in which the fluorine atoms reside only on one sublattice, is not the lowest energy (ground) state of S-FG. [*Ab initio* molecular dynamics simulations of bare and supported S-FG structures were performed using the GGA for the exchange−correlation functional, the projector augmented wave methodology, and a plane-wave basis set with an energy cutoff of 500 eV. For the simulation of free-standing fluorographenes $6 \times 6 \times 1$ supercells were used. For supported structures a 4×4 supercell of fluorographene and corresponding four-layered SiC substrate were considered. The sampling of the Brillouin zone was done for the supercell with the equivalent of a $3 \times 3 \times 1$ Monkhorst−Pack *k*-point grid for these supercells. The simulations were performed within the microcanonical (NVE) ensemble with velocities assigned according to the Maxwell−Boltzmann distribution at the temperature of 500 K during the entire calculation. To avoid large temperature fluctuations, velocities were normalized every 50 steps. The total duration of the simulation was 2 ps with the time step equal to 1 fs. We believe that the methodology of molecular dynamics calculations is good enough to see possible instabilities and bond-breaking processes.] Instead the "boat" (see Figure 2C and D) is the real ground state of S-FG. This is due to the stronger C−F bonds and $\pi-\pi$ interactions between C atoms, which result in a large energy benefit of ∼0.8 eV per F atom.[17] Moreover, all p_z electrons of fluorine-free C atoms are paired, such that no magnetic moments occur. Our DFT calculations give a C−F bond length of 1.41 for the case of hydrogen-intercalated S-FG on SiC(0001), in excellent agreement with the XPD data in Figure 2B.

Conversion of pristine graphene into S-FG is expected to induce massive changes in the valence level electronic structure, and this is borne out by the angle-resolved photoemission data in Figure 3A. First, the linearly dispersing π states that cross at the K point, distinctive of pristine graphene,[32] are removed, and a set of bands extends from about −3.5 eV down to around −12 eV, some of them strongly dispersing in the region from −3.5 to −10 eV. The uppermost bands (∼−2 eV) are quite dispersionless across the entire Brillouin zone. The lower, strongly dispersing, bands are due to the in-plane bonds, and our DFT calculations (shown in red in Figure 3B) demonstrate that the bands are quite different for the chair and boat conformation. First the band gap of the boat phase is considerably larger (although both are underestimated, a common problem with DFT calculations), and second, the chair

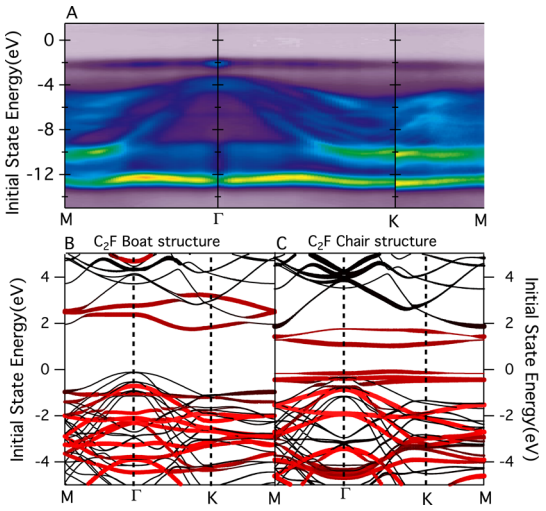

Figure 3. Angle-resolved photoemission images obtained from single-sided fluorinated graphene on H/SiC (A) along the three principal directions, recorded at a photon energy of 95 eV. The linearly dispersing bands of pristine graphene are missing, and a nondispersing peak is observed at ∼−2 eV. This peak increases upon EUV or X-ray irradiation. DFT calculations of the band structure of single-sided fluorographene in the boat (B) and chair (C) structure, exhibiting considerable differences in the size of the fundamental band gap and the nature of the states near the top of the valence band. Black lines are substrate bands, and red lines are from the S-FG, while the thickness of the bands indicates the DOS. Hexagonal symmetry lines are used in all three plots to allow for a direct comparison between the different structures, despite the "boat" structure not being strictly hexagonal.

configuration is characterized by a dispersionless band at about ∼−2 eV, which is well separated from the top of the dispersing valence bands. Our predictions are obtained from first-principles plane-wave calculations within density functional theory, performed using the spin-polarized generalized gradient approximation and projector augmented wave (PAW) potentials. The kinetic energy cutoff for a plane-wave basis set is taken as 500 eV. In the self-consistent potential and total energy calculations of S-FG/H/SiC, a set of $(25 \times 25 \times 1)$ *k*-point samplings is used for Brillouin zone (BZ) integration. The convergence criterion of self-consistent calculations for ionic relaxations is 10^{-5} eV between two consecutive steps. By using the conjugate gradient method, all atomic positions and unit cells are optimized until the atomic forces are less than 0.03 eV/A. Pressures on the lattice unit cell are decreased to values less than 0.5 kbar.

A comparison of the calculated band structure of S-FG and the ARPES data shown in Figure 3 shows that both the boat and chair conformations reproduce major features, especially at higher binding eneriges. The experimental valence band data set in Figure 3A in fact exhibits a ∼−2 eV dispersionless band, and so at first glance one may conclude that our S-FG occurs in the chair conformation; however the situation is more complex. We find that the core and valence band signals change with the amount of exposure to

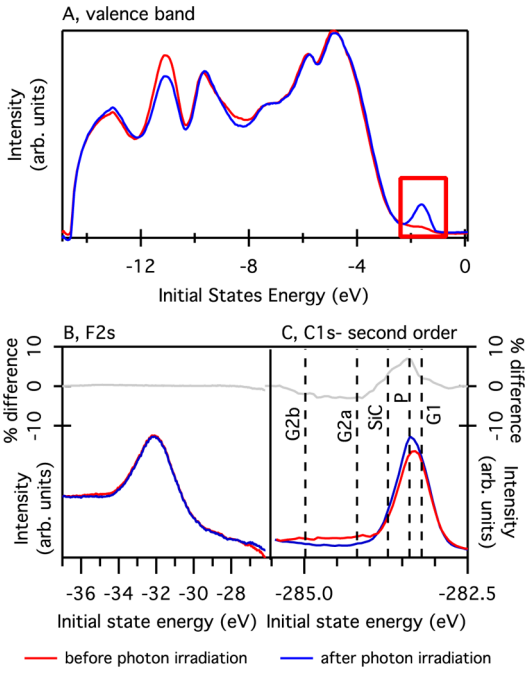

Figure 4. (A) Angle-integrated valence band spectra obtained before (red) and after extended illumination with X-rays. Note the increase of the state at ∼−2 eV upon ilumination (red box). (B) F 2s and C 1s core level spectra taken before (red) and after (blue) X-ray exposure; new features signaling the phase change are obvious on the C 1s core level, while no change occurs on the F 2s level. The use of second-order light to obtain the C 1s spectra and the F 2s peak rather than the F 1s peak was done so that valence bands (in A), fluorine XPS (in B), and C 1s (in C) could all be obtained simultaneously, with the correct choice of scan parameters (photon energy, kinetic energy range, *etc.*).

extreme UV or X-ray photons. The most obvious change is that the intensity of the nondispersive band at ∼−2 eV increases with photon dose. This can be investigated by performing time-dependent measurements of ARPES, XPS, and NEXAFS as a function of photon exposure.

On the basis of such data, we conclude that the ground-state, "boat", conformation is converted to a different phase upon illumination, as evident from the strong increase in the signal in the region marked by the red box in the angle-integrated valence band spectra in Figure 4A. The presence of the ∼−2 eV dispersionless band in Figure 3A is thus inevitable, as the photoemission process implies photon irradiation; time-dependent measurements show the intensity of this state increasing with exposure. This is also reflected in the C 1s core level spectra in Figure 4C, where a change in the line shape (as made clear by the difference curve above the spectra) occurs, while the F 2s line shows no change in the fluorination level. The dotted lines in Figure 4C indicate the peak assignments from Figure 1B. From this we can clearly see that the P line increases, while the G2a and G2b lines decrease with photon exposure. For these measurements the F 2s line and the second-order C 1s line are used, as, with the correct choice of experimental photon energy and kinetic energy range, they can be measured simultaneously with the ARPES spectra. (In our case we used a photon energy of 286 eV, which places the second-order C 1s peak (572 eV photons) ∼3 eV above the Fermi level, and an initial state energy range from −37 to 5 eV.)

The signatures of S-FG in the conduction band investigated by near-edge X-ray absorption fine structure (NEXAFS), Figure 5, also reveal details about the unoccupied bands in both the metastable and ground states and permit an estimation of the magnitude of the band gap. Upon fluorination, the carbon π^* resonance at 285.5 eV is eliminated, consistent with the formation of C−F bonds. The reduction of the graphene (G) peaks and the emergence of new peaks (labeled F-G) demonstrate the massive rearrangement of the electronic structure in the unoccupied states upon fluorination. The emergence of a new antibonding state, at 284.3 eV photon energy, mirrors the EUV-induced nondispersive state (∼−2 eV) in the ARPES data. The inset in Figure 5A shows the area of the 284.3 eV photon energy state taken before and after photon irradiation; it clearly shows that this peak, similar to its occupied counterpart at −2 eV, is also related to the new, photon-induced, metastable phase. Taken together these features provide a massive reduction of the fundamental band gap in S-FG. This is best seen by plotting the occupied density of states (DOS), obtained from angle-integrated photoemission, and the unoccupied states, obtained from NEXAFS, together on an initial state energy scale. For the NEXFAS data, the scale change from kinetic energy to initial state energy involves placing the zero energy at the Fermi level (*i.e.*, subtracting 283.7 eV from the photon energy). The two states related to the metastable photon- induced phase are at −1.9 and 0.6 eV, respectively, giving a band gap of 2.5 eV in the metastable conformation. The next set of states away from the Fermi level are at −4 and 2.2 eV, respectively, indicating that the ground, "boat", configuration has a band gap of roughly 6.2 eV.

The calculations described above indicate that the energy barrier between the "chair" and the "boat" structures is ∼15−20 eV; this therefore provides strong evidence that the UV-induced transition is not a structural change from the "boat" to the "chair" conformation (the energy barrier is too high). We therefore ascribe the metastable state to photon-induced "defects" in the ground "boat" structure. Indeed flat dispersionless bands are well documented for organic thin films, where they are ascribed to highly localized π and π^* states. Our explanation then is that the photon irradiation produces structural defects in the "boat" configuration that lead to localized, non F-bonded, C π and π^* states, which form in the gap of the S-FG "boat" electronic structure. This reduces the band gap from

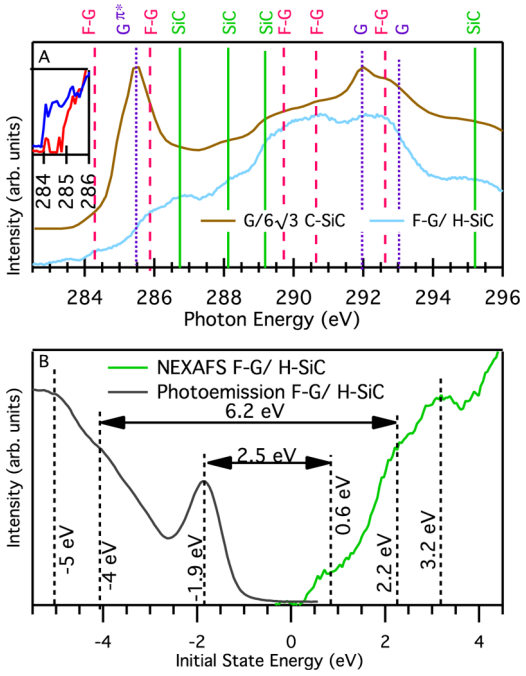

Figure 5. Near-edge X-ray absorption fine structure spectra obtained from SS-FG/H−SiC (light blue) and G/6√3 C−SiC (A) (brown). The absence of the sp^2 ($G^{\pi*}$) peak in the fluorinated graphene indicates that fluorine is bonded to graphene in an sp^3 geometry, consistent with the X-ray photoelectron diffraction measurements (Figure 2). The inset shows the π^* state is absent before (red) and increases upon (blue) irradiation with UV photons. (B) Angle-integrated valence band spectra (gray, negative initial state energy) and near-edge X-ray absorption fine structure spectra (green, positive initial state energy) obtained from fluorinated graphene on H/SiC. The separation of the occupied and unoccupied localized states indicates an insulating sample with a band gap of ~2.5 eV after photon activation and ~6.2 eV before. The designation of peaks due to graphene (G), fluorinated graphene (F-G), and substrate (SiC) is done by comparison with pristine graphene and SiC. In B only the F-G peaks are indicated.

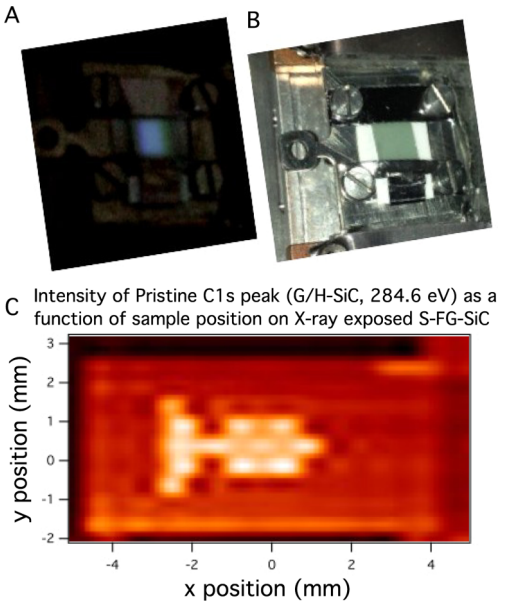

Figure 6. (A) Image of mounted sample emitting blue light under annealing, concurrent with the transition from the metastable conformation to the ground, boat, conformation. The same sample mounted on the sample holder is shown in B for comparison. (C) Real-space scan of the pristine C 1s spectra for G/H-SiC (284.6 eV) of a SS-FG sample that was "patterned" by intense UV light. The "fish" shape in the center of the sample indicates the regions that were patterned and now have the chemical and electronic structure of pristine graphene. The surrounding region consists of SS-FG in the metastable state. Patterning was performed using a spot size of 200 μm.

~6.2 eV to ~2.5 eV and results in an extra "defect" peak (labeled P in Figure 1) in the XPS spectra.

A most intriguing observation that fully supports the above line of reasoning is that the meat-stable defect phase can be converted back to the stable ground state by mild annealing. This process is accompanied by the emission of blue light, which is the color expected from the magnitude of the band gap derived from the data in Figure 5B. Figure 6A shows a sample that is subjected to an ac heating; a blue emission is clearly identified from the UV-exposed region (the sample on its holder in ultrahigh vacuum is shown for comparison in Figure 6B). A similar emission has been observed for samples that were radiatively heated using a filament, and so emission is not an electroluminescent process. In addition this new illumination process results in a decrease of the C 1s core level labeled "P" (see Figure 1A), the 0.6 eV π^* state (see Figure 5A), and the ~−1.9 eV π state (see Figure 3A), a corresponding increase in the C 1s core levels labeled G2a and G2b, but no change in the F 1s core level. This annealing, and subsequent light emission, therefore, converts the sample from the metastable configuration to the ground, "boat", configuration. As further confirmation that the light is emitted from the single monolayer of fluorinated graphene and not from the substrate, the same measurement was performed on clean H-terminated SiC and graphene on H-terminated SiC samples, and no light emission was observed. In addition, this light emission is not observed on S-FG on H-terminated SiC samples that have not been activated by photons (*i.e.*, placed in the metastable configuration) and so is directly related to the transition from the metastable state to the ground state. As a further check, the same process was undertaken with indirect, filament heating, and the emission was still observed. This conclusively rules out the SiC substrate as the source of the emission, as the electroluminescence of the substrate requires a current to be passed through the substrate for the emission to occur.

A further influence of UV or X-ray irradiation that may well be of technological relevance is the fact that upon exposure to extremely intense UV or X-ray light we observe that the F atoms can be removed in a controlled way, creating patterns on the sample, in which the metallic electronic structure of pristine graphene is restored. Such patterning, theoretically predicted for half-hydrogenated graphene,[33,34] is

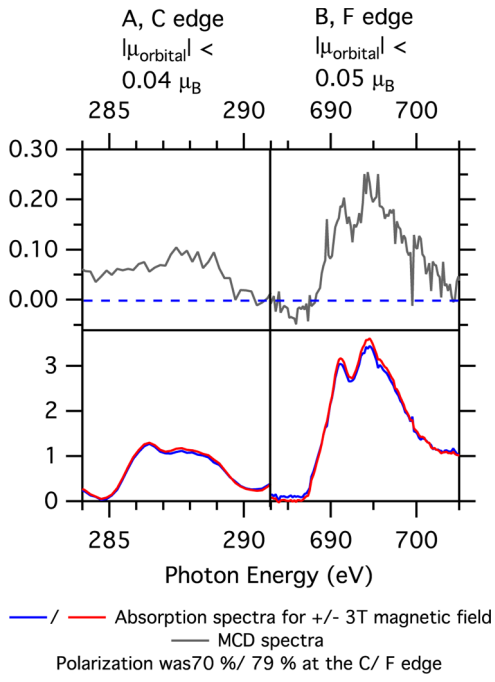

Figure 7. X-ray magnetic circular dichroism (XMCD) measurements obtained at the carbon 1s (~286 eV) and the fluorine 1s (~690 eV) absorption edges on a half-fluorinated graphene on H/SiC sample. A magnetic field strength of 3 T was used, and the sample was cooled to ~20 K. The bottom row shows the absorption spectra taken using 70% (carbon edge) and 79% (fluorine edge) circularly polarized light, for a magnetic field parallel (red) and anti-parallel (blue). The circular dichroism plots are shown in the top row (gray).

shown in Figure 6C. The "fish-shaped" region consists of metallic graphene surrounded by semiconducting S-FG regions. This demonstrates the potential for lithographic patterning of semimetallic regions on a semiconducting sample. That the fluorinated region remains semiconducting in this process, with a low doping, is demonstrated by our observation that charging of the sample is observed in photoemission for temperatures below 70 K, the temperature at which the carriers in the SiC substrate freeze out, which confirms the vanishing density of states at the Fermi level at low temperatures. As a result of this charging problem, the photoemission and LEED data where taken at ~100 K, while the STM measurements where performed at room temperature to avoid sample charging issues.

Hydrogenated and fluorinated graphene have been intensely studied with a view to magnetic properties in metal-free compounds, and the question of whether half-fluorinated graphene exhibits a magnetically ordered phase has been debated (see ref 35 and references therein). Hence we have investigated the possible magnetic properties of half-fluorinated graphene using absorption X-ray magnetic circular dichroism (XMCD) measurements of the C 1s and F 1s edges (Figure 7). These data show no appreciable dichroism signal at temperatures of 10 K and magnetic fields up to 3 T, which indicates a very small orbital long-range ferromagnetic moment. In fact an analysis of the dichroism signals using the methods of Merz *et al.*[36] can give an upper limit to the magnitude of the orbital magnetic moment of 0.04 and 0.05 μ_b for C and F atoms, respectively. (The upper limit to the orbital magnetic moments, $m_{orbital}$, is given by the equation $|m_{orbital}| = (-2/3)(\Delta A_k/A_k)(n_h)$[36], where ΔA_k and A_k are the area of the magnetic dichroism curve and absorption curve integrated over the absorption edge and n_h is the number of holes. In our calculations we use a value of $n_h = 1$, which overestimates the orbital moment.) While a large spin magnetic moment cannot be excluded from these measurements, we found that the ARPES measurements and band structure calculations show that our sample exhibits the boat conformation of SS-FG, which is a nonmagnetic semiconductor.

The intriguing properties of this new material, including luminescence, lithographically patternable metallic regions, and the semiconducting electronic structure, make it an ideal candidate for future graphene-based electronic devices. Combining this with the industrially friendly substrate SiC and a scalable fluorination process increases the technological interest in this new functionalization of graphene.

Conflict of Interest: The authors declare no competing financial interest.

Acknowledgment. The Advanced Light Source is supported by the Director, Office of Science, Office of Basic Energy Sciences, of the U.S. Department of Energy under Contract No. DE-AC02-05CH11231. Work in Erlangen was supported by the ESF and the DFG through the EUROCORES program EUROGRAPHENE. A.L.W. acknowledges support from the Max- Planck-Gesellschaft, the Donostia International Physics Centre, and the Centro de Fisica de Materiales in San Sebastian, Spain. We gratefully acknowledge the Max-Planck Institute for Intelligent Systems Stuttgart for use of their XMCD end station at WERA, and the ANKA Ångströmquelle Karlsruhe for the provision of beamtime. K.J.J. acknowledges support from an INHA University Research Grant (INHA-47292). H.S. and F.M.P. were supported by the Flemish Science Foundation (FWO-Vl), the EUROCORES program EUROGRAPHENE, and the Methusalem Foundation of the Flemish government. Computational resources were provided by TUBITAK ULAKBIM, High Performance and Grid Computing Center (TR-Grid e-Infrastructure), and HPC infrastructure of the University of Antwerp (CalcUA), a division of the Flemish Supercomputer Center (VSC), which is funded by the Hercules Foundation. H.S. is supported by an FWO Pegasus Marie Curie Fellowship.

REFERENCES AND NOTES

1. Novoselov, K. S.; Geim, A. K.; Morozov, S. V.; Jiang, D.; Zhang, Y.; Dubonos, S. V.; Grigorieva, I. V.; Firsov, A. A. Electric Field Effect in Atomically Thin Carbon Films. *Science* **2004**, *306*, 666–669.
2. Geim, A. K.; Novoselov, K. S. The Rise of Graphene. *Nat. Mater.* **2007**, *6*, 183.
3. Bostwick, A.; Ohta, T.; McChesney, J.; Seyller, T.; Rotenberg, E. Renormalization of Graphene Bands by Many-Body Interactions. *Solid State Commun.* **2007**, *143*, 63–71.
4. Zhou, S.; Siegel, D.; Fedorov, A.; Lanzara, A. Metal to Insulator Transition in Epitaxial Graphene Induced by Molecular Doping. *Phys. Rev. Lett.* **2008**, *101*, 086402.

5. Bostwick, A.; McChesney, J.; Emtsev, K.; Seyller, T. Quasiparticle Transformation during a Metal-Insulator Transition in Graphene. *Phys. Rev. Lett.* **2009**, *103*, 056404.
6. Bostwick, A.; Speck, F.; Seyller, T.; Horn, K.; Polini, M.; Asgari, R.; MacDonald, A. H.; Rotenberg, E. Observation of Plasmarons in Quasi-Free-Standing Doped Graphene. *Science* **2010**, *328*, 999–1002.
7. Crassee, I.; Levallois, J.; Walter, A. L.; Ostler, M.; Bostwick, A.; Rotenberg, E.; Seyller, T.; van der Marel, D.; Kuzmenko, A. B. Giant Faraday Rotation in Single- and Multilayer Graphene. *Nat. Phys.* **2010**, *7*, 48–51.
8. Yan, J.; Zhang, Y.; Kim, P.; Pinczuk, A. Electric Field Effect Tuning of Electron-Phonon Coupling in Graphene. *Phys. Rev. Lett.* **2007**, *98*, 166802.
9. Denis, P. Band Gap Opening of Monolayer and Bilayer Graphene Doped with Aluminium, Silicon, Phosphorus and Sulfur. *Chem. Phys. Lett.* **2010**, *492*, 251–257.
10. Rana, F. Graphene Terahertz Plasmon Oscillators. *IEEE Trans. Nanotechnol.* **2008**, *7*, 91–99.
11. Loh, K. P.; Bao, Q.; Eda, G.; Chhowalla, M. Graphene Oxide as a Chemically Tunable Platform for Optical Applications. *Nat. Chem.* **2010**, *2*, 1015–1024.
12. Elias, D. C.; Nair, R. R.; Mohiuddin, T. M. G.; Morozov, S. V.; Blake, P.; Halsall, M. P.; Ferrari, A. C.; Boukhvalov, D. W.; Katsnelson, M. I.; Geim, A. K.; *et al*. Control of Graphene's Properties by Reversible Hydrogenation: Evidence for Graphane. *Science* **2009**, *323*, 610–613.
13. Nair, R. R.; Ren, W.; Jalil, R.; Riaz, I.; Kravets, V. G.; Britnell, L.; Blake, P.; Schedin, F.; Mayorov, A. S.; Yuan, S.; *et al*. Fluorographene: A Two-Dimensional Counterpart of Teflon. *Small* **2010**, *6*, 2877–2884.
14. Jeon, K.-J.; Lee, Z.; Pollak, E.; Moreschini, L.; Bostwick, A.; Park, C.-M.; Mendelsberg, R.; Radmilovic, V.; Kostecki, R.; Richardson, T. J.; *et al*. Fluorographene: A Wide Bandgap Semiconductor with Ultraviolet Luminescence. *ACS Nano* **2011**, *5*, 1042–1046.
15. Lee, W. H.; Suk, J. W.; Chou, H.; Lee, J.; Hao, Y.; Wu, Y.; Piner, R.; Akinwande, D.; Kim, K. S.; Ruoff, R. S. Selective-Area Fluorination of Graphene with Fluoropolymer and Laser Irradiation. *Nano Lett.* **2012**, *12*, 2374–2378.
16. Sato, Y.; Itoh, K.; Hagiwara, R.; Fukunaga, T.; Ito, Y. On the So-Called "Semi-Ionic" C–F Bond Character in Fluorine–GIC. *Carbon* **2004**, *42*, 3243–3249.
17. Şahin, H.; Topsakal, M.; Ciraci, S. Structures of Fluorinated Graphene and their Signatures. *Phys. Rev. B* **2011**, *83*, 115432.
18. Cheng, S. H.; Zou, K.; Okino, F.; Gutierrez, H. R.; Gupta, A.; Shen, N.; Eklund, P. C.; Sofo, J. O.; Zhu, J. Reversible Fluorination of Graphene: Evidence of a Two-Dimensional Wide Bandgap Semiconductor. *Phys. Rev. B* **2010**, *81*, 205435.
19. Gong, P.; Wang, Z.; Wang, J.; Wang, H.; Li, Z.; Fan, Z.; Xu, Y.; Han, X.; Yang, S. One-Pot Sonochemical Preparation of Fluorographene and Selective Tuning of its Fluorine Coverage. *J. Mater. Chem.* **2012**, *22*, 16950.
20. Zhou, J.; Liang, Q.; Dong, J. Enhanced Spin-Orbit Coupling in Hydrogenated and Fluorinated Graphene. *Carbon* **2010**, *48*, 1405–1409.
21. Zhou, J.; Wu, M. M.; Zhou, X.; Sun, Q. Tuning Electronic and Magnetic Properties of Graphene by Surface Modification. *Appl. Phys. Lett.* **2009**, *95*, 103108.
22. Junkermeier, C. E.; Badescu, S. C.; Reinecke, T. L. Highly Fluorinated Graphene. *Arxiv Prepr.* **2013**, *1302*, 6878v1.
23. Emtsev, K.; Speck, F.; Seyller, T.; Ley, L.; Riley, J. Interaction, Growth, and Ordering of Epitaxial Graphene on SiC 0001 Surfaces: A Comparative Photoelectron Spectroscopy Study. *Phys. Rev. B* **2008**, *77*, 155303.
24. Riedl, C.; Coletti, C.; Iwasaki, T.; Zakharov, A. A.; Starke, U. Quasi-Free-Standing Epitaxial Graphene on SiC Obtained by Hydrogen Intercalation. *Phys. Rev. Lett.* **2009**, *103*, 246804.
25. Mcfeely, F.; Morar, J.; Shinn, N.; Landgren, G.; Himpsel, F. Synchrotron Photoemission Investigation of the Initial Stages of Fluorine Attack on Si Surfaces: Relative Abundance of Fluorosilyl Species. *Phys. Rev. B* **1984**, *30*, 764–770.
26. Withers, F.; Dubois, M.; Savchenko, A. Electron Properties of Fluorinated Single-Layer Graphene Transistors. *Phys. Rev. B* **2010**, *82*, 073403.
27. Robinson, J. T.; Burgess, J. S.; Junkermeier, C. E.; Badescu, S. C.; Reinecke, T. L.; Perkins, F. K.; Zalalutdniov, M. K.; Baldwin, J. W.; Culbertson, J. C.; Sheehan, P. E.; *et al*. Properties of Fluorinated Graphene Films. *Nano Lett.* **2010**, *10*, 3001–3005.
28. Speck, F.; Ostler, M.; Röhrl, J.; Jobst, J.; Waldmann, D.; Hundhausen, M.; Ley, L.; Weber, H. B.; Seyller, T. Quasi-Freestanding Graphene on SiC (0001). *Mater. Sci. Forum* **2010**, *645*, 629–632.
29. Yeh, J. J.; Lindau, I. Atomic Subshell Photoionization Cross Sections and Asymmetry Parameters: $1 < Z < 103$. *Atomic Data and Nuclear Data Tables*; Academic Press: New York, 1985; Vol. 32.
30. Ohta, T.; Bostwick, A.; McChesney, J.; Seyller, T.; Horn, K. Interlayer Interaction and Electronic Screening in Multilayer Graphene Investigated with Angle Resolved Photoemission Spectroscopy. *Phys. Rev. Lett.* **2007**, *98*, 206802.
31. Wu, M.; Liu, E.-Z.; Jiang, J. Z. Magnetic Behavior of Graphene Absorbed with N, O, and F Atoms: A First-Principles Study. *Appl. Phys. Lett.* **2008**, *93*, 082504–082504–3.
32. Bostwick, A.; Ohta, T.; Seyller, T.; Horn, K.; Rotenberg, E. Quasiparticle Dynamics in Graphene. *Nat. Phys.* **2006**, *3*, 36–40.
33. Hernandez-Nieves, A. D.; Partoens, B.; Peeters, F. M. Electronic and Magnetic Properties of Superlattices of Graphene/Graphane Nanoribbons with Different Edge Hydrogenation. *Phys. Rev. B* **2010**, *82*, 165412.
34. Ao, Z. M.; Hernandez-Nieves, A. D.; Peeters, F. M.; Li, S. Enhanced Stability of Hydrogen Atoms at the Graphene/Graphane Interface of Nanoribbons. *Appl. Phys. Lett.* **2010**, *97*, 233109.
35. Ma, Y.; Dai, Y.; Guo, M.; Niu, C.; Yu, L.; Huang, B. Strain-Induced Magnetic Transitions in Half-Fluorinated Single Layers of BN, GaN and Graphene. *Nanoscale* **2011**, *3*, 2301–2306.
36. Merz, M.; Nagel, P.; Pinta, C.; Samartsev, A.; von Löhneysen, H.; Wissinger, M.; Uebe, S.; Assmann, A.; Fuchs, D.; Schuppler, S. X-ray Absorption and Magnetic Circular Dichroism of $LaCoO_3$, $La_{0.7}Ce_{0.3}CoO_3$, and $La_{0.7}Sr_{0.3}Co_3$ Films: Evidence for Cobalt-Valence-Dependent Magnetism. *Phys. Rev. B* **2010**, *82*, 174416.